The Astrophysical Journal, 676:1029–1039, 2008 April 1

INFRARED AND X-RAY EVIDENCE FOR CIRCUMSTELLAR GRAIN DESTRUCTION BY THE BLAST WAVE OF SUPERNOVA 1987A

Eli Dwek,[1] Richard G. Arendt,[2] Patrice Bouchet,[3] David N. Burrows,[4] Peter Challis,[5] I. John Danziger,[6] James M. De Buizer,[7] Robert D. Gehrz,[8] Robert P. Kirshner,[5] Richard McCray,[9] Sangwook Park,[4] Elisha F. Polomski,[8] and Charles E. Woodward[8]

Received 2007 September 21; accepted 2007 December 17

ABSTRACT

Multiwavelength observations of supernova remnant 1987A show that its morphology and luminosity are rapidly changing at X-ray, optical, infrared (IR), and radio wavelengths as the blast wave from the explosion expands into the circumstellar equatorial ring, produced by mass loss from the progenitor star. The observed IR radiation arises from the interaction of dust grains that formed in mass outflow with the soft X-ray-emitting plasma component of the shocked gas. *Spitzer* Infrared Spectrograph spectra at 5–30 μm taken on day 6190 since the explosion show that the emission arises from $\sim 1.1 \times 10^{-6}\ M_{\odot}$ of silicate grains radiating at a temperature of $\sim 180^{+20}_{-15}$ K. Subsequent observations on day 7137 show that the IR flux had increased by a factor of 2 while maintaining an almost identical spectral shape. The observed IR-to-X-ray flux ratio (IRX) is consistent with that of a dusty plasma with standard Large Magellanic Cloud dust abundances. IRX has decreased by a factor of $\sim$2 between days 6190 and 7137, providing the first direct observation of the ongoing destruction of dust in an expanding supernova blast wave on dynamic timescales. Detailed models consistent with the observed dust temperature, the ionization timescale of the soft X-ray emission component, and the evolution of IRX suggest that the radiating silicate grains are immersed in a 3.5×10^6 K plasma with a density of $(0.3\text{–}1) \times 10^4$ cm^{-3} and have a size distribution that is confined to a narrow range of radii between 0.023 and 0.22 μm. Smaller grains may have been evaporated by the initial UV flash from the supernova.

Subject headings: dust, extinction — infrared: general — ISM: individual (SNR 1987A) — supernova remnants — X-rays: general

1. INTRODUCTION

On 1987 February 23, supernova (SN) 1987A, the brightest SN since Kepler's SN in 1604, exploded in the Large Magellanic Cloud (LMC). About 10 years thereafter, the energy output from the SN became dominated by the interaction of its blast wave with the inner equatorial ring (ER), a dense ring of gas located at a distance of about 0.7 lt-yr from the center of the explosion, believed to be produced by mass loss from the progenitor star. The ER is being repeatedly observed at optical wavelengths with the *Hubble Space Telescope* (*HST*; Pun et al. 2002), at X-ray energies with *Chandra* (Park et al. 2006, 2007), at radio frequencies with the Australian Telescope Compact Array (Manchester et al. 2005), and in the mid-IR with the Gemini South Observatory (Bouchet et al. 2004, 2006) and *Spitzer* (Bouchet et al. 2004; Dwek & Arendt 2007). The morphological changes in its appearance in these different wavelength regimes (presented in Fig. 6 of McCray 2007) reveal the progressive interaction of the SN blast wave with the ER. The interaction regions appear as hot spots in the *HST* images, representing the shocked regions of fingerlike protrusions that were generated by Rayleigh-Taylor instabilities in the interaction of the wind from the progenitor star with the ER (see Fig. 2 in McCray 2007).

The X-ray emission is thermal emission from the very hot plasma and consists of two main characteristic components: a hard ($kT \approx 2$ keV) component representing a fast shock propagating into a low-density medium and a soft ($kT \approx 0.3$ keV) component representing a decelerated shock propagating into the denser protrusions (Park et al. 2007; Zhekov et al. 2006). The optical emission arises from the gas that is shocked by the blast wave transmitted through the dense protrusions in the ER (Pun et al. 2002), and the radio emission is synchrotron radiation from electrons accelerated by the reverse shock (Manchester et al. 2005). The mid-IR emission spectrum is comprised of line and continuum emission. The lines most probably originate from the optically bright dense knots. The continuum that dominates the spectrum is thermal emission from dust that was formed in the post-main-sequence wind of the progenitor star before it exploded. This dust could either be located in the shocked X-ray-emitting plasma and heated by electronic collisions or be located in the optical knots and radiatively heated by the shocks giving rise to the optical emission (Polomski et al. 2004; Bouchet et al. 2006). Dust has also formed in the ejecta of the SN about 530 days after the explosion, as evidenced by optical and IR observations of SN 1987A (Lucy et al. 1991; Gehrz & Ney 1990; Moseley et al. 1989; Wooden et al. 1993), but its current contribution to the total mid-IR emission is negligible (Bouchet et al. 2004).

Because the Gemini 11.7 μm image correlates well with both the X-ray and optical emission, the possibility that the dust is radiatively heated in the knots was considered in detail by Bouchet et al. (2006). Estimated dust temperatures of $\sim$125 K fell short of the observed value of $\sim$180 K, but given the uncertainties in the

[1] Observational Cosmology Laboratory, Code 665, NASA Goddard Space Flight Center, Greenbelt, MD 20771; eli.dwek@nasa.gov.
[2] Science Systems and Applications, Inc. (SSAI), Code 665, NASA Goddard Space Flight Center, Greenbelt, MD 20771.
[3] DSM/DAPNIA/Service d'Astrophysique, CEA/Saclay, F-91191 Gif-sur-Yvette, France; Patrice.Bouchet@cea.fr.
[4] Department of Astronomy and Astrophysics, Pennsylvania State University, 525 Davey Laboratory, University Park, PA 16802.
[5] Harvard-Smithsonian Center for Astrophysics, 60 Garden Street, MS-19, Cambridge, MA 02138.
[6] Osservatorio Astronomico di Trieste, Via Tiepolo 11, Trieste, Italy.
[7] Gemini Observatory, Southern Operations Center, c/o AURA, Casilla 603, La Serena, Chile.
[8] Department of Astronomy, University of Minnesota, 116 Church Street SE, Minneapolis, MN 55455.
[9] JILA, University of Colorado, Boulder, CO 80309-0440.

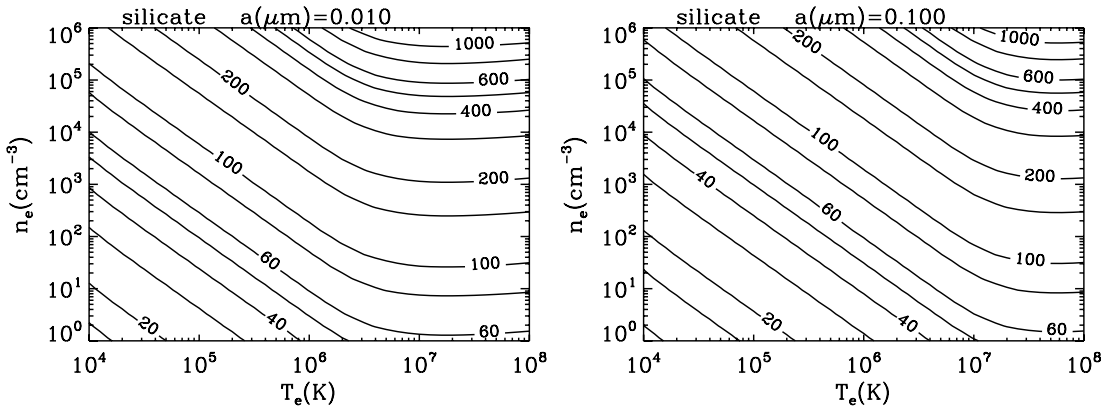

FIG. 1.—Contour plot of the equilibrium temperature of 0.01 (*left*) and 0.10 μm (*right*) silicate grains as a function of electron density and temperature. Above temperatures of $\sim 5 \times 10^6$ K ($\sim 3 \times 10^7$ K), the 0.01 μm (0.1 μm) grains become transparent to the incident electrons, and the dust temperature is only a function of electron density. At lower temperatures, different combinations of plasma density and temperature can heat the dust to the same temperature. We note here that a similar figure (Fig. 15 in Bouchet et al. 2006) was mislabeled and actually corresponds to contour levels of silicate dust temperature for grain radius of $a = 0.0030$ μm.

model parameters, this discrepancy could not firmly rule out this possible scenario for the location and heating mechanism of the dust. However, the combined IR and X-ray observations can be more readily explained if the dust resides in the shocked regions of the fingerlike protrusions that give rise to the observed soft X-ray emission (Zhekov et al. 2006). We will adopt this scenario as our working hypothesis and derive a self-consistent model for the composition, abundance, and size distribution of the dust to explain the evolutionary changes in the IR and X-ray fluxes resulting from the collisional heating and the destruction of the dust grains by the ambient plasma.

We first review the basic physical principles that determine the temperature of collisionally heated dust and describe how the IR emission can be used to probe the physical condition of the X-ray-emitting plasma. We also discuss what information can be derived from the comparison of the IR and X-ray fluxes from the gas (§ 2.1). The physics of dust particles in a hot gas is discussed in more detail by Dwek (1987) and Dwek & Arendt (1992). In § 3 we present a simple analytical model for the evolution of the grain size distribution and total dust mass in the gas that is swept up by an expanding SN blast wave. In § 4 we present *Spitzer* low-resolution 5–30 μm Infrared Spectrograph (IRS) spectra obtained on days 6190 and 7137 after the explosion. The IR spectra are used to derive the temperature and composition of the shock-heated dust. We use IR and X-ray observations of the SN to constrain the grain size distribution and the time at which the SN blast wave first crashed into its dusty surroundings. The results of our paper are summarized in § 5.

2. THE IR DIAGNOSTICS OF A DUSTY X-RAY PLASMA

The morphological similarity between the X-ray and mid-IR images of SN 1987A suggests that the IR emission arises from dust that is collisionally heated by the X-ray-emitting gas. Simple arguments presented below show that, under certain conditions, the IR luminosity and spectrum of a dusty plasma can be used as a diagnostic for the physical conditions of the gas and the details of the gas-grain interactions. Details of the arguments can be found in Dwek (1987) and Dwek & Arendt (1992).

2.1. *The Dust Temperature as a Diagnostic of Electron Density*

The collisional heating rate, $\mathcal{H}$ (erg s^{-1}), of a dust grain of radius a embedded in a hot plasma is given by

$$\mathcal{H} = \pi a^2 \sum_j n_j v_j \mathcal{E}_j, \tag{1}$$

where n_j is the number density of the jth plasma constituent, v_j is its thermal velocity, and $\mathcal{E}_j$ is its thermally averaged energy deposition in the dust. In all the following, we assume that the ion and electron temperatures are equal. Then $v_e \gg v_{\rm ion}$, and the dust heating rate is dominated by electronic collisions.

Let $E_{\rm dep}$ be the thermally averaged energy deposited by electrons in the solid. If most electrons are stopped in the dust, then $E_{\rm dep}$ is, on average, equal to the thermal energy of the electrons, that is, $E_{\rm dep} \propto T_e$, where T_e is the electron temperature. On the other hand, if most incident electrons go entirely through the grains, then $E_{\rm dep}$ is proportional to the electron stopping power in the solid, defined as $\rho^{-1}(dE/dx)$. At the energies of interest here, the electronic stopping power has an energy dependence of $(dE/dx) \sim E^{-1/2}$ (Iskef et al. 1983) or $dE \sim E^{-1/2}\,dx$, so that $E_{\rm dep} \sim T_e^{-1/2} a$.

The functional dependence of the grain heating rate on gas density and temperature is then given by

$$\mathcal{H} \sim \begin{cases} a^2 n_e T_e^{3/2}, & \text{electrons stopped in grain,} \\ a^3 n_e, & \text{electrons go through grain,} \end{cases} \tag{2}$$

where we used the fact that $v_e \sim T_e^{1/2}$. The radiative cooling rate, $\mathcal{L}$ (erg s^{-1}), of the dust grain with temperature T_d by IR emission is given by

$$\mathcal{L} = \pi a^2 \sigma T_d^4 \langle Q \rangle \sim \pi a^3 \sigma T_d^{4+\beta}, \tag{3}$$

where σ is the Stefan-Boltzmann constant and $\langle Q \rangle \propto a T_d^{\beta}$ is the Planck-averaged value of the dust emissivity, $Q(\lambda) \propto \lambda^{-\beta}$, where the value of the emissivity index, β, is $\approx$1–2.

In equilibrium, $\mathcal{H} = \mathcal{L}$, and the dust temperature dependence on plasma density and temperature can be written as

$$T_d \sim \begin{cases} \left(\dfrac{n_e}{a}\right)^{\gamma} T_e^{3\gamma/2}, & \text{electrons stopped in grain,} \\ n_e^{\gamma}, & \text{electrons go through grain,} \end{cases} \tag{4}$$

where $\gamma \equiv 1/(4+\beta)$. These simple arguments show that when the gas temperature is sufficiently high and the grain size sufficiently small so that most electrons go through the grain, the dust temperature depends only on the plasma density.

Figure 1 depicts contour levels of the dust temperature as a function of electron density and temperature for 0.01 and 0.10 μm silicate grains. The figure shows that above a certain gas temperature, the value of which depends on the grain radius, most of the

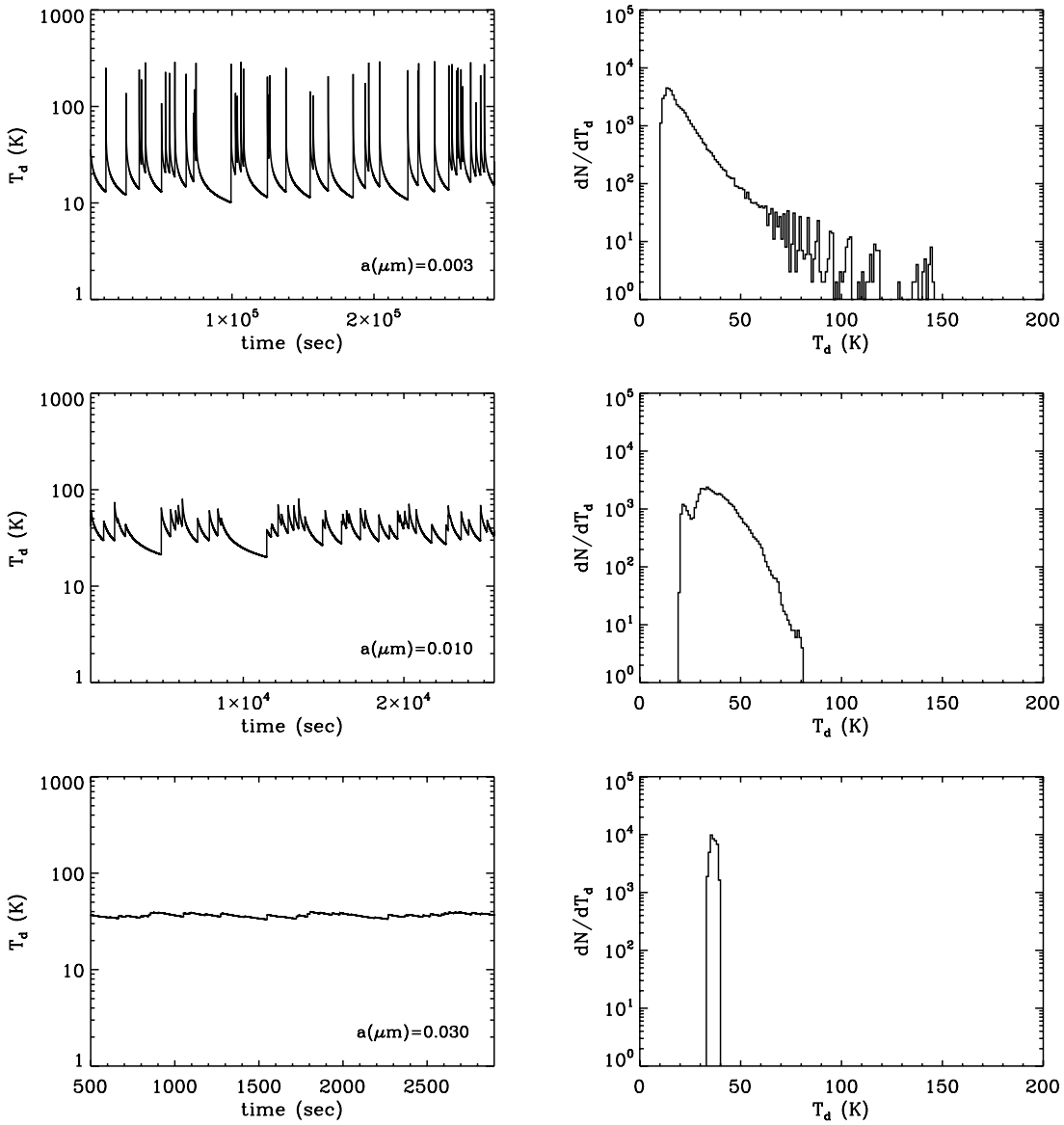

FIG. 2.—Stochastic heating of silicate grains in a hot X-ray-emitting gas characterized by a temperature of $T_g = 10^6$ K and electron density of $n_e = 1$ cm^{-3} for dust grains of different radii. *Left*: Temperature fluctuations as a function of time. *Right*: Histogram of the fluctuations. As the grain size increases, the fluctuations get smaller, and the probability distribution of dust temperatures becomes strongly peaked around the equilibrium temperature of ~38 K.

electrons go through the grain and the dust temperature is essentially determined by the electron density. Under these conditions, the IR spectrum from the collisionally heated grains becomes an excellent diagnostic of the density of the X-ray-emitting gas. However, when the grains are large enough to stop the electrons, the dust temperature only constrains the possible combinations of plasma temperature and density.

2.2. *The Stochastic Heating of Grains by Electronic Collisions*

When dust grains are sufficiently small, a single electronic collision can deposit an amount of energy in the dust that is significantly larger than its enthalpy, causing a surge in dust temperature. If, additionally, the time interval between successive electronic collisions is larger than the dust cooling time, the grain temperature will be fluctuating with time (Dwek 1987; Dwek & Arendt 1992). Figure 2 depicts a simulation of the stochastic heating of 0.003, 0.01, and 0.03 μm silicate grains immersed in a hot X-ray-emitting gas characterized by a temperature $T_g = 10^6$ K and an electron density $n_e = 1$ cm^{-3}. The left column of Figure 2 shows the temperature fluctuations as a function of time, and the right column shows the histogram of the grain temperature. As the grain size increases, the fluctuations get smaller, and the histogram becomes strongly peaked around the equilibrium dust temperature of ~38 K in this example.

2.3. *The IR-to-X-Ray Flux Ratio*

Another important diagnostic of a dusty plasma is IRX, defined as the ratio of the IR to X-ray fluxes emitted by the gas (Dwek 1987). If the dust is collisionally heated by the gas, then the total IR flux, $F_{\rm IR}$, emitted from a gas volume V is proportional to $n_e n_d \Lambda_d(T_g) V$, where n_d is the number density of dust particles and $\Lambda_d(T_g)$ is the cooling function (units of erg cm^3 s^{-1}) of the gas via gas-grain collisions. The total X-ray flux, $F_{\rm X}$, from the same volume is proportional to $n_e^2 \Lambda_g(T_g) V$, where $\Lambda_g(T_g)$ is the cooling function of the gas via atomic processes. Thus,

$$\mathrm{IRX} \equiv \left(\frac{n_d}{n_e}\right) \frac{\Lambda_d(T_g)}{\Lambda_g(T_g)}. \quad (5)$$

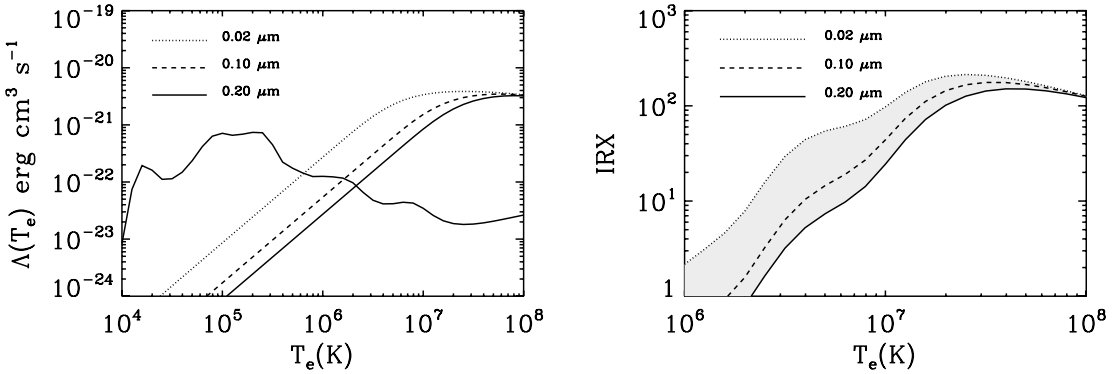

FIG. 3.—*Left*: Cooling function of a dusty plasma via atomic processes (*thick solid line*) and via gas-grain collisions. Calculations were performed assuming a single-sized population of 0.02 (*dotted line*), 0.10 (*dashed line*), and 0.20 μm grains (*solid line*) with a dust-to-gas mass ratio of 0.0062, which is the value in the local ISM of the bare silicate-graphite+PAH dust model of Zubko et al. (2004). The gas cooling rate per unit volume for both processes is given by $L = n_e^2 \Lambda(T)$. *Right*: Value of IRX for single-sized dust populations with radii of 0.02, 0.10, and 0.20 μm with the same dust-to-gas mass ratio as the left panel.

Both cooling functions represent the energy losses through collisional processes, characterized by $\langle \sigma v E \rangle$ summed over all interactions in the plasma, where σ is the cross section, v is the relative velocity of colliding species, and E is the energy lost in the process.

For a given dust-to-gas mass ratio, that is, a fixed (n_d/n_e) ratio, IRX depends only on plasma temperature. Figure 3 (*left*) shows the behavior of the atomic cooling function of a gas of solar composition as a function of gas temperature. Also shown in the figure is the gas cooling function via gas-grain collisions for a gas with a dust-to-gas mass ratio $Z_d = 0.0062$ (Zubko et al. 2004) and single-sized dust populations with radii of 0.02, 0.1, and 0.2 μm. The right panel of Figure 3 presents the value of IRX for the same conditions. The figure shows that for soft X-rays ($kT_e \sim$ 0.3 keV, $T_e \sim 3.5 \times 10^6$ K) this ratio varies between $\sim$3 and 20, depending on grain size. Each plasma temperature will have a different range of values, depending on the grain size distribution. Any deviation from these values will suggest that Z_d is either depleted or overabundant with respect to the reference value adopted in the calculations.

2.4. *The Plasma Ionization Timescale*

The cooling rate of a plasma depends on the ionization state of its constituent ions which may not have evolved to equilibrium conditions. The ionization state of the gas is characterized by the ionization timescale, $\mathcal{F}$ (units of cm^{-3} s), defined as $\mathcal{F} \equiv n_e t_e$, where t_e is the age of the shocked gas. In a fully ionized plasma with $n_e \approx n_{\rm ion}$, $\mathcal{F}$ also measures the fluence of ions incident on the dust. When sputtering is the dominant grain destruction mechanism, $\mathcal{F}$ will directly determine the total mass of dust that is returned to the gas. In summary, the key parameters, plasma temperature, density, ionization timescale, and X-ray fluxes and the dust temperature, grain size distribution, composition, and IR fluxes, are closely interrelated so that knowledge of some parameters will constrain the others.

3. THE EVOLUTION OF THE GRAIN SIZE DISTRIBUTION AND DUST MASS

Consider the propagation of a shock into a dusty medium with a constant number density and a fixed dust-to-gas mass ratio Z_d^0. The shocked gas can be regarded as a reservoir that is continuously being filled with gas and preexistent circumstellar dust by the expanding blast wave. If dust grains were not destroyed, the postshock gas would maintain a constant value Z_d^0 as the mass of shocked dust and gas evolve proportionally in time, with a functional dependence that depends on the geometry of the medium into which the blast wave is expanding. In the case where dust particles are destroyed by sputtering, the grain size distribution and the dust-to-gas mass ratio in the shocked gas will evolve with time.

3.1. *General Equations*

A grain of radius a_0 that is swept up by the shock at some time t_0 will at time t be eroded to a radius $a(t)$ given by

$$a \equiv a(t) = a_0 + \int_{t_0}^{t} \left(\frac{da}{dt'} \right) dt', \tag{6}$$

where

$$\frac{da}{dt} \sim \sum_j n_j v_j Y_j < 0, \tag{7}$$

where Y_j is the thermally averaged sputtering yield of the dust by the jth gas constituent.

Dust particles swept up by a high-velocity shock will move ballistically through the shock front and acquire a velocity relative to the shocked gas. The sputtering yield then needs to be averaged over a Maxwellian distribution of velocities that is displaced by the relative gas-grain motion from its origin in velocity space (Dwek & Arendt 1992). Figure 4 shows the temperature dependence of the sputtering rate of silicate dust grains, calculated using

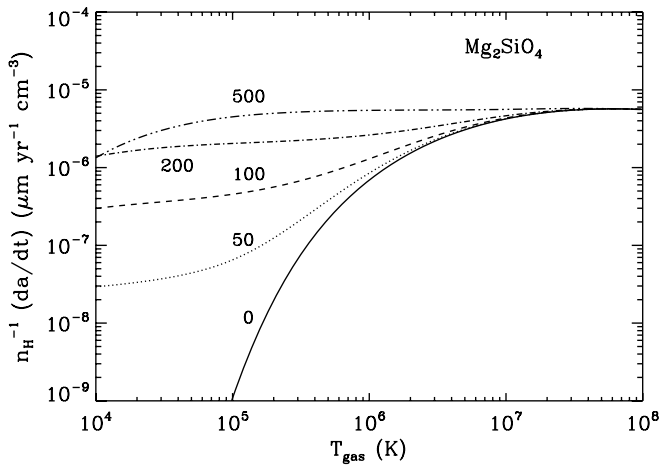

FIG. 4.—Absolute value of the sputtering rate (normalized to the H number density) of silicate (Mg_2SiO_4) dust grains moving through a hot gas of solar composition as a function of gas temperature. The lines are marked by the grain velocity (in km s^{-1}).

sputtering yield parameters given by Nozawa et al. (2006), moving with velocity $v_{\rm gr} = 0, 50, 100, 200$, and 500 km s^{-1} through a hot gas of solar composition. In contrast to the heating of grains, their erosion by thermal and kinetic sputtering is entirely done by the ionic constituents of the gas. For dust grains with velocities $\gtrsim$500 km s^{-1} and gas temperatures above $\sim 10^6$ K, the sputtering rate is approximately constant and given by

$$\frac{da}{dt} \approx -5 \times 10^{-6} n_{\rm H}\left({\rm cm}^{-3}\right)\ \mu{\rm m\ yr}^{-1}. \tag{8}$$

Equation (8) ignores the possible destruction of grains by evaporative grain-grain collisions that occurs in slower ($\lesssim$100 km s^{-1}) shocks by the acceleration of charged grains with MHD turbulence (Yan et al. 2004).

If the shocked gas maintains a constant composition and density, then a dust grain of initial radius a_0 that is swept up by the shock at some time t' will at time t have a radius a given by

$$a = a_0 + \left(\frac{da}{dt}\right)(t - t'). \tag{9}$$

Equation (9) can be written in dimensionless form as

$$\xi = \xi_0 - \frac{(t - t')}{\tau_{\rm max}} = \xi_0 - (\eta - \eta'), \tag{10}$$

where $\xi \equiv a/a_{\rm max}$, $\xi_0 \equiv a_0/a_{\rm max}$, $\eta \equiv t/\tau_{\rm max}$, $\eta' \equiv t'/\tau_{\rm max}$, and

$$\tau_{\rm max} \equiv a_{\rm max}|da/dt|^{-1} \tag{11}$$

is the sputtering lifetime of the largest grain in the injected size distribution, which (using eq. [8]) is numerically given by

$$\begin{aligned}\tau_{\rm max} &= 2 \times 10^5\, \frac{a_{\rm max}(\mu{\rm m})}{n_{\rm H}({\rm cm}^{-3})}\ {\rm yr} \\ &= 7.3 \times 10^7\, \frac{a_{\rm max}(\mu{\rm m})}{n_{\rm H}({\rm cm}^{-3})}\ {\rm days}.\end{aligned} \tag{12}$$

Let n_d be the total number density of dust grains in the preshocked gas, and let $n_d(a_0)da_0$ be the number density of grains with radii between a_0 and $a_0 + da_0$. We assume that the grains have a size distribution in the preshocked gas given by

$$n_d = \int_0^\infty n_d(a_0)da_0 \equiv n_d \int_0^\infty f(a_0)da_0, \tag{13}$$

where $f(a_0)$ is the normalized size distribution. If the grain size distribution extends over a limited range of radii, $a_{\rm min} \le a_0 \le a_{\rm max}$, then $f(a_0) = 0$ for any $a_0 < a_{\rm min}$ or $a_0 > a_{\rm max}$.

Dust grains are continuously injected into the shocked gas by the expanding SN blast wave. The total number of shocked grains with radii a in the $[a, a + da]$ interval at time t, $N_d(a, t)da$, is equal to the number of all dust particles of initial radius a_0 that were swept up at time t' ($0 \le t' \le t$) and sputtered during the time interval t'–t to radius a given by equation (9). If $\dot{V}(t)$ is the growth rate of the volume of the shocked gas, then $N_d(a, t)$ can be written as

$$N_d(a, t) = n_d \int_0^t \dot{V}(t')f(a_0)dt'. \tag{14}$$

The lower limit of the integral, $t = 0$, corresponds to the time when the blast wave first encounters the dusty medium. The total mass of shocked dust at any given time t is given by

$$M_d(t) = \int_{a_{\rm min} - |da/dt|t}^{a_{\rm max}} m_d(a)N_d(a, t)da, \tag{15}$$

where $m_d(a) = 4\pi\rho a^3/3$ is the mass of a dust grain of radius a. Equation (14) can be written in dimensionless form as

$$N_d(\xi, \eta) = n_d \int_0^\eta \left[\frac{dV(\eta'\tau_{\rm max})}{d\eta'}\right] f[(\xi + \eta - \eta')a_{\rm max}]d\eta'. \tag{16}$$

This integral is a convolution of the form $g(\eta') * f(\eta_0 - \eta')$, which can be numerically evaluated for arbitrary functions using Fourier transforms.

3.2. *A Simple Analytical Solution*

An analytical solution can be derived for a preshocked grain size distribution given by a power law in grain radius and a power-law time dependence of $\dot{V}$. We write the grain size distribution as

$$f(a_0) = \begin{cases} \mathcal{C}a_0^{-k}, & a_{\rm min} \le a_0 \le a_{\rm max}, \\ 0, & \text{otherwise}, \end{cases} \tag{17}$$

where $\mathcal{C} \equiv (k - 1)/(a_{\rm min}^{-k+1} - a_{\rm max}^{-k+1})$ is the normalization constant. The time dependence of $\dot{V}(t')$ can be written as

$$\dot{V}(t') = \dot{V}_0 \left(\frac{t'}{\tau_{\rm max}}\right)^\alpha, \tag{18}$$

where $\dot{V}_0$ is a proportionality constant, $\alpha = 2$ for a spherical blast wave expanding into a uniform interstellar medium (ISM), and $\alpha = 0$ if the blast wave expands into a one-dimensional "finger-like" protrusion.

The total number density of grains in the $[a, a + da]$ radius interval is then given by

$$N_d(a, t) = n_d \dot{V}_0 \int_0^t \left(\frac{t'}{\tau_{\rm max}}\right)^\alpha f(a_0)dt'. \tag{19}$$

Using equation (9) to change variables from t' to a_0, equation (19) can be rewritten as

$$\begin{aligned}N_d(a, t) = \dot{N}_d &\left|\frac{da}{dt}\right|^{-1} \mathcal{C} \\ &\times \int_{a_{\rm low}}^{a_{\rm up}} \left[\left(\frac{t}{\tau_{\rm max}} + \frac{a}{a_{\rm max}}\right) - \left(\frac{a_0}{a_{\rm max}}\right)\right]^\alpha a_0^{-k}\, da_0,\end{aligned} \tag{20}$$

where $\dot{N}_d \equiv n_d \dot{V}_0$.

The time dependence of $N_d(a, t)$ is contained in the limits on the integral over the grain size distribution. If the radius a is within the range of the injected grain size distribution, that is, $a_{\rm min} \le a \le a_{\rm max}$, then $a_{\rm low} = a$, since only grains with radii larger than a could have contributed to $N_d(a, t)$. If the radius a is smaller than $a_{\rm min}$, then $N_d(a, t)$ is nonzero only if $a + |da/dt|t$ exceeds $a_{\rm min}$, and $a_{\rm low} = a_{\rm min}$. In other words, the most recent injection of grains that could have contributed to $N_d(a, t)$ occurred at time $t - \Delta t$, where Δt is the time required to reduce the grain radius from $a_{\rm min}$ to a. The largest grains that could have been sputtered

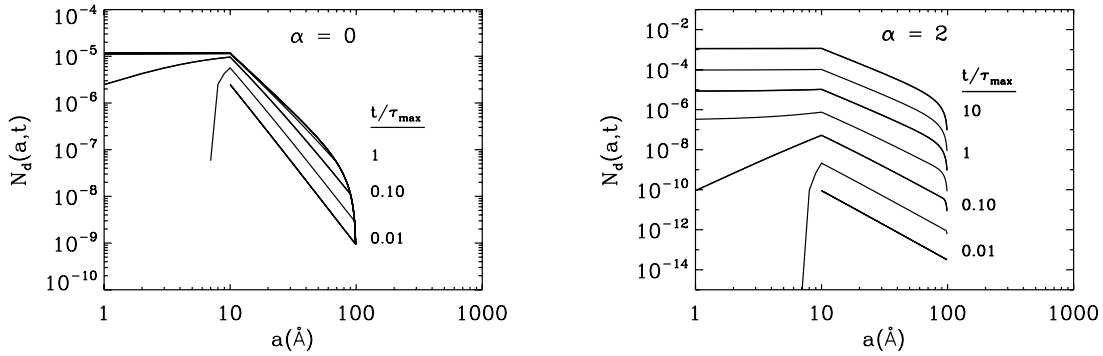

FIG. 5.—Evolution of the grain size distribution with time, measured in units of $\tau_{\max}$, the sputtering lifetime of the largest grain with radius $a_{\max}$ in the size distribution. Calculations were performed for a grain size distribution characterized by an $\sim a^{-3.5}$ power law in grain radii between 10 and 100 Å. The grain destruction rate, da/dt, was taken to be 0.14 Å day^{-1}, for an assumed density of 10^4 cm^{-3}. Thick lines are labeled by $t/\tau_{\max}$. *Left*: Spherical blast wave expanding into a one-dimensional protrusion ($\alpha = 0$). *Right*: Spherical blast wave expanding into a uniform ISM ($\alpha = 2$).

to radius a during the time t is equal to $a + |da/dt|t$. However, the largest grain size cannot exceed $a_{\max}$, so the upper limit on the integral, $a_{\rm up}$, is determined by the smaller of these two quantities. To summarize,

$$a_{\rm low} = \max(a_{\min}, a),$$
$$a_{\rm up} = \min\left(a_{\max}, a + \left|\frac{da}{dt}\right| t\right). \tag{21}$$

For a spherical shock wave expanding into a one-dimensional protrusion ($\alpha = 0$), the solution to equation (20) is given by

$$N_d(a,t)_{\alpha=0} = \dot{N}_d \left|\frac{da}{dt}\right|^{-1} \frac{\mathcal{C}}{(k-1)} \left(a_{\rm low}^{-k+1} - a_{\rm up}^{-k+1}\right). \tag{22}$$

At early times, when $t < a|da/dt|^{-1} \ll \tau_{\max}$, $a_{\rm up} = a$, and $a_{\rm low} \approx a$, the solution to equation (22) becomes

$$N_d(a,t)_{\alpha=0} = \dot{N}_d t \mathcal{C} a^{-k}. \tag{23}$$

At late times, when $t > \tau_{\max}$ and $a_{\rm up} = a_{\max}$, the asymptotic solution of equation (22) is

$$N_d(a, t > \tau_{\max})_{\alpha=0} = \begin{cases} \dot{N}_d \left|\dfrac{da}{dt}\right|^{-1} \dfrac{\mathcal{C}}{(k-1)} \left(a^{-k+1} - a_{\max}^{-k+1}\right), & a > a_{\min}, \\ \dot{N}_d \left|\dfrac{da}{dt}\right|^{-1} \dfrac{\mathcal{C}}{(k-1)} \left(a_{\min}^{-k+1} - a_{\max}^{-k+1}\right) = \text{const}, & a \le a_{\min}. \end{cases} \tag{24}$$

For a shock wave expanding into a homogeneous medium ($\alpha = 2$), the solution is given by

$$N_d(a,t)_{\alpha=2} = \dot{N}_d \left|\frac{da}{dt}\right|^{-1} \mathcal{C} \left[\frac{1}{(k-1)} \left(\frac{t}{\tau_{\max}} + \frac{a}{a_{\max}}\right)^2 \times \left(a_{\rm low}^{-k+1} - a_{\rm up}^{-k+1}\right) - \frac{2}{(k-2)} \left(\frac{t}{\tau_{\max}} + \frac{a}{a_{\max}}\right) \times \left(\frac{a_{\rm low}^{-k+2} - a_{\rm up}^{-k+2}}{a_{\max}}\right) + \frac{1}{(k-3)} \left(\frac{a_{\rm low}^{-k+3} - a_{\rm up}^{-k+3}}{a_{\max}^2}\right)\right]. \tag{25}$$

At late times, when $t \gg \tau_{\max}$, the first term dominates, and the asymptotic solution of equation (25) increases with time as t^2,

$$N_d(a, t > \tau_{\max})_{\alpha=2} = \dot{N}_d \left|\frac{da}{dt}\right|^{-1} \frac{\mathcal{C}}{(k-1)} \left(\frac{t}{\tau_{\max}}\right)^2 \mathcal{G}(a,t), \tag{26}$$

where

$$\mathcal{G}(a,t) \equiv \begin{cases} a^{-k+1} - a_{\max}^{-k+1}, & a > a_{\min}, \\ a_{\min}^{-k+1} - a_{\max}^{-k+1} = \text{const}, & a \le a_{\min}. \end{cases} \tag{27}$$

Figure 5 depicts the grain size distribution for different epochs. Select epochs, labeled by the dimensionless quantity $t/\tau_{\max}$, are represented by thick lines. Calculations were performed for an initial grain size distribution characterized by an $\sim a^{-3.5}$ power law in grain radius between 10 and 100 Å. The grain destruction rate, $|da/dt|$, was taken to be 0.14 Å day^{-1}, calculated for the sputtering rate of silicate grains in a hot gas with a temperature and density of $\sim 10^6$–10^8 K and 1000 cm^{-3}, respectively.

Figure 5 illustrates the dependence of the evolution of the grain size distribution on the geometry of the ISM into which the blast wave is expanding. For a one-dimensional protrusion ($\alpha = 0$), Figure 5 (*left*) shows a clear convergence of the size distribution to a fixed functional form and total number of grains for $t/\tau_{\max} \gtrsim 1$. As the shock wave expands, the thickness of the shell of swept-up dust increases with time. However, because of the finite grain lifetime, its thickness cannot exceed a value of $\Delta R_{\rm sh} \approx v_{\rm sh}\tau_{\max}$, where $v_{\rm sh}$ is the shock velocity. So, the grain size distribution and total mass reaches a steady state limit. When the blast wave expands into a uniform medium, the shell of shocked dust reaches the same steady state thickness $\Delta R_{\rm sh}$. However, since the surface of the shell increases as $R_{\rm sh}^2$, where $R_{\rm sh}$ is the radius of the blast wave, the mass of shocked gas will continue to increase. This is clearly depicted in Figure 5 (*right*), which shows that $N_d(a,t)$ reaches a steady state, but continues to increase with time as t^2.

If grains were not sputtered in the shocked gas, then $N_d^0(a,t)da$, the total number of dust grains in the $[a, a + da]$ radius interval that are swept up by the shock at time t, would be

$$N_d^0(a,t)da = \dot{N}_d \tau_{\max} \frac{\mathcal{C}}{(\alpha+1)} \left(\frac{t}{\tau_{\max}}\right)^{\alpha+1} a^{-k}\, da. \tag{28}$$

Their mass, M_d^0, is given by equation (15) with $N_d(a,t)$ replaced by the expression above and with $|da/dt|$ set to zero.

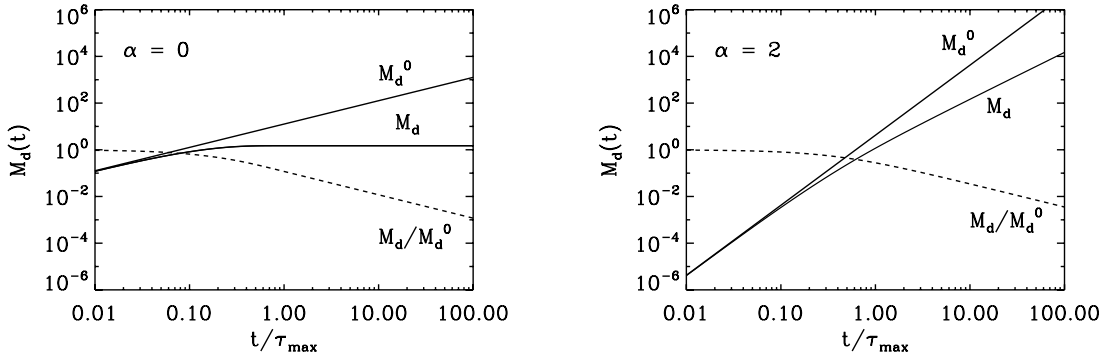

FIG. 6.—Evolution of the dust mass M_d, the dust mass if grains were not sputtered M_d^0, and the fraction of the surviving dust M_d/M_d^0 with time, measured in units of $\tau_{\rm max}$, the sputtering lifetime of the largest grain in the size distribution [$\tau_{\rm max}({\rm days}) = 7.3 \times 10^7 a_{\rm max}(\mu{\rm m})/n_{\rm H}({\rm cm}^{-3})$]. Dust and gas parameters are identical to those used in Fig. 5. The figure shows that the fractional change in M_d/M_d^0 between two epochs constrains the grain size distribution and the density of the X-ray-emitting plasma. The fraction M_d/M_d^0 is proportional to IRX, the IR-to-X-ray flux ratio of the shocked gas. *Left*: Spherical blast wave expanding into a one-dimensional protrusion ($\alpha = 0$). *Right*: Spherical blast wave expanding into a uniform ISM ($\alpha = 2$).

Figure 6 shows the evolution of dust mass for a spherical blast wave expanding into a one-dimensional protrusion ($\alpha = 0$; *left*) and into a uniform ISM ($\alpha = 2$; *right*) as a function of $t/\tau_{\rm max}$. As explained above, when $\alpha = 0$ the mass of shocked dust, M_d, reaches a constant limit for $t \gg \tau_{\rm max}$; whereas for $\alpha = 2$, the mass of the shocked dust will increase as t^2. If grains were not destroyed, the mass of swept-up dust, M_d^0, would increase as t for $\alpha = 0$ and as t^3 for $\alpha = 2$. Figure 6 also shows the evolution of the mass fraction of surviving dust grains, M_d/M_d^0. This mass fraction is proportional to the dust-to-gas mass ratio in the shocked gas, and for a constant gas temperature and density, it is also proportional to IRX, the IR-to-X-ray flux ratio in the shocked gas. Figure 6 shows that the fractional change in M_d/M_d^0 between two epochs constrains the value of $\tau_{\rm max}$ given in equation (12) which in turn depends on the grain size distribution and the density of the X-ray-emitting plasma. As a reminder, $\tau_{\rm max}({\rm days}) = 7000 a_{\rm max}(\text{Å})/n_{\rm H}({\rm cm}^{-3})$. For example, given a plasma density the value of $\tau_{\rm max}$ will depend only on $a_{\rm max}$, the maximum grain radius. A small value of $a_{\rm max}$ will imply a low value for $\tau_{\rm max}$, so that large changes in M_d/M_d^0 occur over very short timescales. Conversely, large values of $a_{\rm max}$ and $\tau_{\rm max}$ will cause changes in M_d/M_d^0 to occur over very long timescales.

4. *Spitzer* IR OBSERVATIONS OF SNR 1987A

4.1. *The Evolution of the IR Spectrum*

Figure 7 shows the 5–30 μm low-resolution spectra of SNR 1987A taken on 2004 February 4 (day 6190 since the explosion), and on 2006 September 8 (day 7137 since the explosion) with the IRS (Houck et al. 2004a, 2004b) on board the *Spitzer Space Telescope* (Werner et al. 2004; Gehrz et al. 2007). Analysis of the spectrum taken on day 6190 revealed that the IR emission originated from $\sim 1.1 \times 10^{-6}\ M_\odot$ of silicate grains radiating at a temperature of $\sim 180^{+20}_{-15}$ K (Bouchet et al. 2006). These circumstellar grains were formed in the quiescent outflow of the progenitor star before it exploded. The total IR flux on day 6190 was 5.1×10^{-12} erg cm^{-2} s^{-1} (Bouchet et al. 2006) and increased after 947 days (day 7137) to 10.0×10^{-12} erg cm^{-2} s^{-1}. The right panel of Figure 7 presents a comparison between the two spectra, both normalized to the same 10 μm intensity. The figure shows that the spectra are essentially identical, implying that the dust composition and temperature remained unchanged during the two observing periods. The line near the bottom in Figure 7 is the ratio between the two spectra, emphasizing their similarity. The IR intensity increased by a factor of 2 between the two epochs.

4.2. *Determining the Grain Size Distribution*

The size distribution of collisionally heated dust grains is constrained by the combinations of gas temperature and density that can give rise to the range of observed dust temperatures. The temperature of the gas giving rise to the soft X-ray component can be derived from models and is equal to $\sim$0.3 keV ($T_e = 3.5 \times 10^6$ K; Park et al. 2005), narrowing down the range of viable plasma densities and grain sizes.

Figure 8 depicts contours of the dust temperature as a function of gas density and grain size for the given electron temperature,

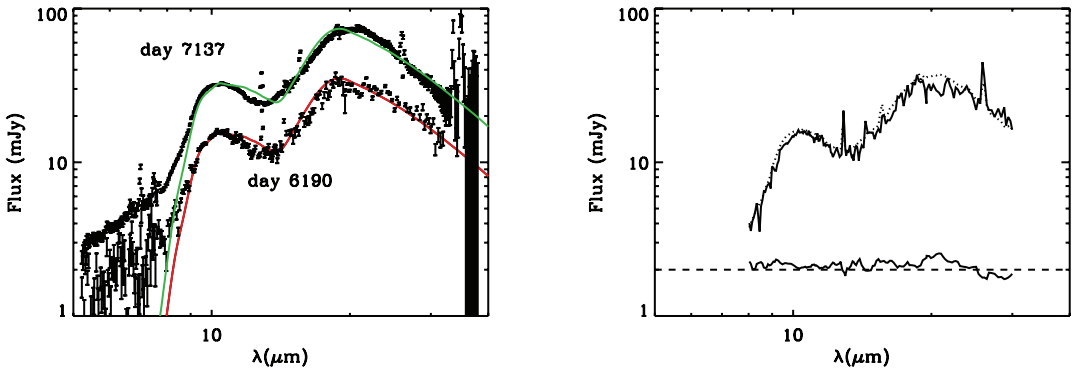

FIG. 7.—*Left*: Evolution of the IR spectrum of SN 1987A from 2004 April 2 (day 6190 since the explosion) to 2006 September 8 (day 7137) taken with the *Spitzer* IRS (Bouchet et al. 2006). *Right*: Smoothed spectra for days 6190 (*solid line*) and 7137 (*dashed line*), normalized to the same brightness. The solid line near the bottom shows the ratio between the two spectra, with the horizontal line being the mean value. The figure shows that the dust spectrum increased by a factor of 2 between the two epochs, retaining essentially an identical spectrum corresponding to silicate grains radiating at an equilibrium temperature of 180^{+20}_{-15} K.

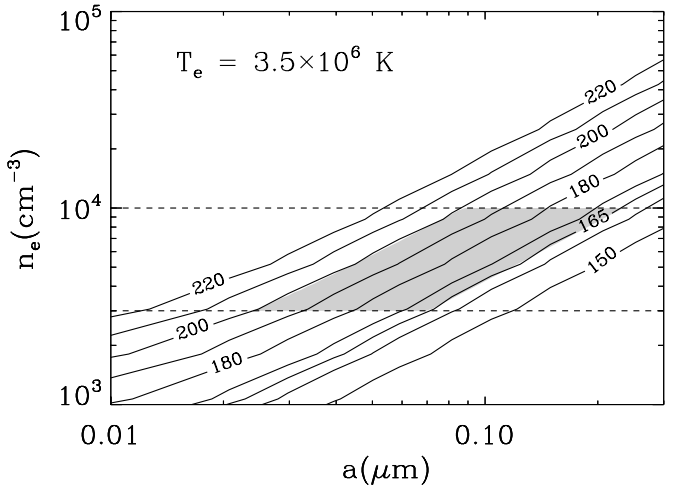

FIG. 8.—Contours of the dust temperature as a function of gas density and grain size for the given electron temperature, T_e, of the soft X-ray component. For the range of electron densities constrained by the plasma ionization timescale (indicated by the dashed horizontal lines), the observed range of dust temperature (indicated by the thick contours) limits the grain size distribution to be between ~0.023 and 0.22 μm.

$T_e = 3.5 \times 10^6$ K. The range of observed dust temperature falls between 165 and 200 K, and the figure shows the different combinations of grain size and gas density that can give rise to this narrow range of dust temperature. All grain sizes are viable, provided that the gas density has the right value to heat the dust to the observed range of temperatures. However, the range of viable grain sizes can be narrowed down by using the constraints on the ionization timescale of the plasma.

The ionization timescale derived from modeling the soft X-ray spectra taken on days 6914, 7095, and 7271 is given by $\mathcal{F} = n_e t_e \gtrsim 10^7$ cm^{-3} days (Park et al. 2007). The ionization time, t_e, is constrained by the time t_0 when the SN blast wave first encountered the ER. Observationally, we can associate t_0 with the appearance of the first hot spot in the *HST* image from 1997 April, about 3700 days after the explosion (Pun et al. 2002). The soft X-ray light curve shows that the rise could have occurred between days 3700 and 6000. The first epoch corresponds to the first appearance of the optical knots, and the latter epoch corresponds to the time when the flux from the soft X-ray component ($kT \sim$ 0.3 keV) exceeded that from the hard component ($kT \sim 2$ keV; Park et al. 2005). From the mid-IR light curves (Bouchet et al. 2006), the energy output from the SN became ER dominated around day 4000. Adopting days 4000–6000 as a reasonable estimate for t_0 gives a range of possible ionization times of $t_e \approx 7000 - t_0 \approx 1000$–$3000$ days. Using the constraints on $\mathcal{F}$, the corresponding limits on the electron densities are $n_e \approx 10^4$ to 3×10^3 cm^{-3}.

These densities are high enough that even small dust grains with radii ~10 Å will be collisionally heated to their equilibrium dust temperature. Furthermore, for a gas temperature of $T_e \approx 3.5 \times 10^6$ K, an equilibrium temperature of ~180 K can only be reached at these high densities if the soft X-ray electrons are stopped in the grains (see Fig. 4). The narrow range of grain temperatures then suggests that the grain size distribution should have a narrow range as well, since $T_d \sim a^{-\gamma}$ (see eq. [4]). Figure 8 shows that the constraint on the electron density, $n_e \approx (0.3$–$1) \times 10^4$ cm^{-3}, limits the range of viable grain sizes that can be heated up to $T_d \approx 165$–200 K to be between 0.023 and 0.22 μm. This range is narrower than that adopted by Weingartner & Draine (2001) to model the size distribution of LMC silicate dust (see their § 4.7).

The smaller upper limit on the size distribution of the silicates in the ER may be limited by the nucleation timescale in the outflow of the SN 1987A progenitor. The higher lower limit on the silicate size distribution in the ER may be the result of evaporation by the initial UV flash (see § 4.3). *HST* images of the ER show that it is located at a distance of ~0.7 lt-yr (6.6×10^{17} cm) from the SN. At this distance, small dust particles can be evaporated by the initial UV flash that emanated from the SN (Fischera et al. 2002). Their calculations suggest that silicate dust particles with radii less than ~0.02 μm will be evaporated by the flash. A population of silicate grains with a $a^{-3.5}$ power-law distribution in grain radius extending from 10 Å to 0.2 μm will lose about 30% of its mass.

4.3. *The Value of* IRX*: Constraining the Dust Abundance in the ER*

A comparison of the IR and X-ray fluxes provides strong constraints on the dust abundance in the shocked gas. X-ray fluxes taken between days 6157 and 7271 with *Chandra* (Park et al. 2007) were interpolated for days 6190 and 7137 of the *Spitzer* observations. The total X-ray flux on day 6190, corrected for an extinction H column density of $N_{\rm H} = 2.35 \times 10^{21}$ cm^{-2}, is 2.1×10^{-12} erg cm^{-2} s^{-1}, half of it radiated by the slow shock component (Park et al. 2005). The IR emission originates from the slow shock component which is penetrating the denser regions of the ER. This component comprises half of the observed X-ray flux. The resulting value of IRX on day 6190 is therefore 4.9 ± 1.1.

The theoretical value for IRX in a gas with LMC ISM abundances, taken here to be 0.6 times solar (Welty et al. 1999), ranges from about 2 to 12 for soft X-rays with $T_e \sim 3 \times 10^6$ K. The dust abundance in the ER is therefore consistent with LMC abundances. Since the silicon abundance in the ER should not have been altered by stellar nucleosynthesis, this agreement suggests efficient condensation of silicate grains in the pre-SN outflow. The dust abundance on day 6190 is a lower limit on the original pre-SN value, since some of the dust may have been evaporated by the initial UV flash from the SN.

4.4. *The Evolution of* IRX

4.4.1. *Evidence for Ongoing Grain Destruction by the SN Blast Wave*

In § 3 we consider the propagation of a shock into a dusty medium with a constant number density and a fixed dust-to-gas mass ratio. If dust grains were not destroyed, then postshock gas would maintain a constant dust-to-gas mass ratio, and the X-ray and IR fluxes from the shocked gas will evolve proportionally in time, that is, the value of IRX will remain constant. Any evolution in the value of IRX should therefore suggest a breakdown in the assumptions of the model.

Observational evidence, summarized in Table 1, shows that the IR flux increased by only a factor of ~2 from day 6190 to 7137. In comparison, the extinction-corrected 0.50–2.0 keV flux increased by a factor of ~3 during the same time period to a value of $\sim 6.4 \times 10^{-12}$ erg cm^{-2} s^{-1} (Park et al. 2007). The fractional contribution of the soft X-ray component increased from 0.5 to 0.6, with no significant change in gas temperature ($kT \sim$ 0.3 keV). All the increase in the soft X-ray flux can therefore be ascribed to an increase in the volume of the dense ($n_e \sim 10^4$ cm^{-3}) component of the ER that was shocked by the SN blast wave. The evolution in the X-ray and IR fluxes and the resulting value of IRX are summarized in Table 1. A similar evolutionary trend

TABLE 1
OBSERVED X-RAY AND IR FLUXES FROM SN 1987A

Days[1]	X-Ray Flux[2]	$f_{\rm soft}$[3]	IR Flux	IRX Flux Ratio[4]
6190.....	$(2.1 \pm 0.32) \times 10^{-12}$	0.50	$(5.1 \pm 0.9) \times 10^{-12}$	4.9 ± 1.1
7137.....	$(6.4 \pm 0.32) \times 10^{-12}$	0.60	$(1.0 \pm 0.18) \times 10^{-11}$	2.6 ± 0.5

NOTE.—Fluxes are in units of erg cm^{-2} s^{-1}.
[1] Since the explosion.
[2] X-ray flux in the 0.5–2.0 keV band, interpolated to the epochs of the *Spitzer* observations and corrected for an extinction column density of $N_{\rm H} = 2.35 \times 10^{21}$ cm^{-2}. The error represents the uncertainty in the pile-up correction factor (Park et al. 2007).
[3] The fraction of the 0.5–2.0 keV flux that arises from the soft ($kT \sim 0.3$ keV) X-ray component (Park et al. 2005).
[4] The ratio of the IR to soft X-ray flux from the SN. The value of IRX has decreased by a factor of 0.53 ± 0.16 from day 6190 to day 7137.

was reported by Bouchet et al. (2004, 2006) although absolute values of IRX differ from those reported here because of differences in the X-ray energy bandpasses and dust models used in the calculations.

If grains were not destroyed, we would expect the IR intensity to increase by a similar factor. The smaller increase in the IR flux, that is, the decline in IRX, is a strong indicator that *we are for the first time witnessing the actual destruction of dust in a shock on a dynamical timescale*. If the dust composition and size distribution is uniform throughout the region of the ER that has been swept up by the shock, then IRX is directly proportional to the dust-to-gas mass ratio, Z_d, or to M_d/M_d^0, the ratio between the actual mass of dust in the shocked gas and the dust mass if grains were not destroyed. The magnitude of the decrease in IRX between the two epochs is strongly determined by the following factors: (1) the grain size distribution in the preshocked gas of the ER; (2) the density of the X-ray-emitting gas and the grain destruction efficiency, which determine the *rate* of grain destruction; and (3) the total time the dust is exposed to the flux of ions, which is determined by the time the SN blast wave first crashed into the ER. The latter factor determines the *total* mass of dust that is returned to the gas.

The dependence of the evolution of IRX on the grain size distribution is somewhat subtle. If the preshocked grain sizes are too large, then the fractional mass of the dust that could be destroyed during the time interval of 947 days will be too small to account for the observed decrease in the value of IRX. Conversely, if the grain sizes were too small, most of the dust mass would be destroyed, giving rise to a significantly larger than observed decrease in IRX between the two epochs. The right combination of grain sizes, gas density, and ion exposure time is therefore required to produce the observed dust temperature and decrease in IRX.

4.4.2. *The Grain Destruction Rate in the Hot Plasma*

Figure 9 depicts the evolution in the IRX(t_2)/IRX(t_1) ratio as a function of $t_1 - t_0$, where t_0 is the time since the explosion when the SN blast wave first crashed into the dense material of the ER, taken here to be the independent variable. The times $t_1 =$ 6190 days and $t_2 = 7137$ days correspond to the two epochs of near-simultaneous *Spitzer* and *Chandra* observations of the ER. The IRX(t_2)/IRX(t_1) ratio is derived by taking the ratio of the fraction of the surviving dust mass, M_d/M_d^0, at the epochs $t_2 - t_0$ and $t_1 - t_0$ (see Fig. 6). Implicit in Figure 9 is a conversion from the dimensionless time variable $t/\tau_{\rm max}$ to absolute time.

The observed IRX(t_2)/IRX(t_1) ratio is $\sim 0.53 \pm 0.16$ (see Table 1) and is shown as a horizontal dashed line in Figure 9. The grain size distribution used in the calculations is characterized by a $a^{-3.5}$ power law in grain radii, extending from a minimum grain size of 10 Å to a value of $a_{\rm max}$ of 0.01, 0.04, and 0.1 μm. Results are presented for a SN blast wave expanding into a one-dimensional protrusion ($\alpha = 0$; Fig. 9, *left column*) and a uniform medium ($\alpha = 2$; Fig. 9, *right column*) with densities of 10^3 cm^{-3} (Fig. 9, *top row*) and 10^4 cm^{-3} (Fig. 9, *bottom row*). The red lines in the two bottom panels correspond to calculations performed for the grain size distribution of the ER with $[a_{\rm min}, a_{\rm max}] = [0.023, 0.22]$ μm.

Figure 9 shows that the IRX(t_2)/IRX(t_1) ratio attains its lowest value when $t_1 - t_0$ is small, that is, when the first encounter of the ER with the SN blast wave occurred just before t_1, the first epoch of *Spitzer* observations. Since t_1 is very close to t_0, very little grain destruction could have taken place during the $t_1 - t_0$ epoch. The value of IRX(t_1) is therefore close to its preshock value. Consequently, any subsequent destruction would lead to relatively great changes in IRX at $t = t_2$. Conversely, IRX(t_2)/IRX(t_1) attains its largest value when $t_0 = 0$ (a physical impossibility because of the finite time required for the SN blast wave to reach the ER). Then, the relative change in IRX between the two epochs will be the smallest, and IRX(t_2)/IRX(t_1) $\rightarrow 1$. To illustrate the asymptotic behavior of the ratio of IRX values, the lines were drawn for $t_1 - t_0$ values beyond the maximum physical value of 6137 days.

Figure 9 also shows the implicit dependence of the IRX(t_2)/IRX(t_1) ratio on the grain destruction rate. When $\tau_{\rm max}$ is small compared to the timescale of blast wave–ER interaction, the grain size distribution relaxes to its equilibrium form, and the lines of IRX(t_2)/IRX(t_1) for the different grain size distributions converge to the same functional form at sufficiently large values of $t_1 - t_0$. This is especially evident in the bottom two panels of Figure 9, for which the gas density is higher, and grain destruction timescales are lower. At $t_1 - t_0 \gtrsim 1000$ days, the lines of IRX(t_2)/IRX(t_1) for the different size distributions have all converged to the same functional form.

Figure 9 shows that the value of $t_1 - t_0$ ranges from $\approx$500 to 2000 days, for IRX(t_2)/IRX(t_1) $= 0.53 \pm 0.16$, giving values of $t_0 \approx 5700$–4200 days for $\alpha = 0$. The range of values for t_0 is consistent with the uncertainties in the time of the blast wave encounter with the ring. This suggests that the grain size distribution derived from the X-ray constraint on the ionization timescale, the range of plasma densities, and the grain destruction efficiency used in the model are all consistent with the observed evolution of IRX and the estimated epoch of the first interaction of the blast wave with the ER.

The problem can also be reversed to determine the grain destruction efficiency by thermal sputtering, by adopting the epoch of $t_0 = 4000$ days and the nominal value of IRX(t_2)/IRX(t_1) $=$ 0.53 as accurate descriptions of the encounter time and the rate of decrease in IRX in the 6190–7137 time interval. The value of

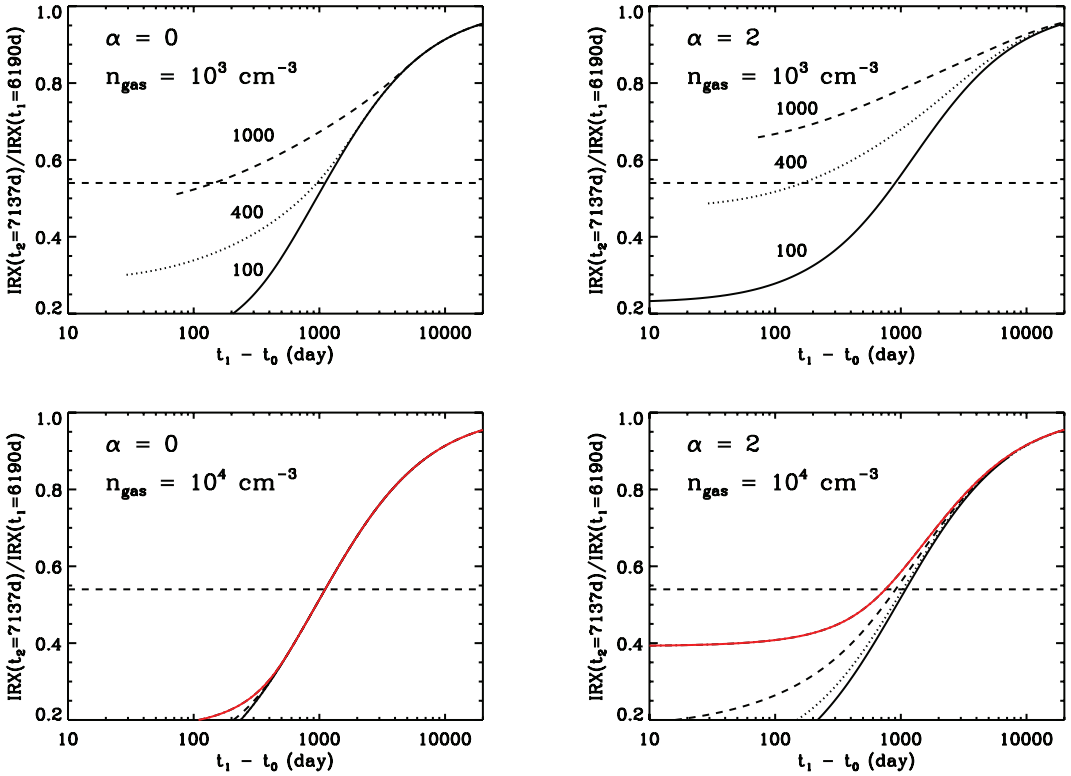

FIG. 9.—Evolution of the ratio IRX(t_2)/IRX(t_1) as a function of the time difference $t_1 - t_0$. The time t_0 is the time since the explosion when the SN blast wave first encountered the dusty equatorial ring (ER), taken here to be the independent variable. The times t_1 and t_2 correspond, respectively, to days 6190 and 7137 since the explosion, the two epochs of near-simultaneous *Spitzer* and *Chandra* observations of the ER. The dashed horizontal line depicts the nominal value of the IRX(t_2)/IRX(t_1) ratio which is 0.53 ± 0.16 (see Table 1). The lines are labeled by $a_{\rm max}$, the maximum grain size (in Å) of the distribution. The minimum grain size was taken to be 10 Å in all cases. The red lines correspond to a narrow grain size distribution of the ER with $[a_{\rm min}, a_{\rm max}] = [0.023, 0.22]$ μm. Panels are also labeled by the value of $n_{\rm gas}$, the density of the shocked gas. *Left*: Spherical blast wave expanding into a one-dimensional protrusion ($\alpha = 0$). *Right*: Spherical blast wave expanding into a uniform ISM ($\alpha = 2$).

$\tau_{\rm max}$ then needs to be adjusted to move the intercept from the calculated value of $t_1 - t_0 \approx 1000$ days to the desired value of $\sim$2000 days. This will require an increase in $\tau_{\rm max}$ by a factor of 2 or a *decrease* in the destruction rate of the silicate grains by a factor of $\sim$2.

4.5. *Implications for Determining the Mass of the Circumstellar Environment of* SN 1987A *Using Light Echoes*

It is interesting to compare the dust properties derived for the ER with those derived for the progenitor's circumstellar environment from studies of the evolution and intensity of light echoes created by the scattering of the optical light from the SN by the dust grains. At any given time, all points with equal delay time lie on an ellipsoid of revolution with the SN at one focal point and the observer at the other. Unfortunately, the ellipsoid at the earliest epoch at which the echoes were observed was outside the ER (see Fig. 11 in Sugerman et al. 2005a). As a result, the light echoes probed only the circumstellar and interstellar media exterior to the ER.

Assuming cylindrical and reflection symmetry, Sugerman et al. (2005b, 2005a) derived a model for the morphology of the scattering medium consisting of: (1) a peanut-shaped contact discontinuity (CD) between the red supergiant and main-sequence winds from the progenitor star; (2) a structure called Napoleon's Hat (NH) constituting the waist of this peanut; and (3) the two outer rings of the circumstellar shell (CS) that define the hourglass that is pinched by the ER. To model the scattered light, Sugerman et al. (2005b, 2005a) used the Weingartner & Draine (2001) model for interstellar LMC dust with grain radii ranging from an upper limit of 0.2–2.0 μm to a lower limit of 0.00035 μm. By varying the relative silicate-to-carbon dust mass ratio while maintaining an LMC dust-to-gas mass ratio that is 0.3 times the value of the local ISM, they estimated a total nebular mass of 1.7 $M_\odot$. They also found that the gas density increases, the maximum grain size decreases, and the silicate-to-carbon dust mass ratio increases as the echo samples material that is closer to the SN. The ER, with its population of smaller pure silicate grains, is consistent with this trend. The higher value of the minimum grain size in the ER may be the result of its proximity to the SN which caused the evaporation of grains smaller than 0.02 μm by the initial UV flash. Finally, the dust abundance in the ER is consistent with that adopted by Sugerman et al. (2005a) for the nebula, supporting their derived value for the nebular mass.

5. SUMMARY

The interaction of the SN 1987A blast wave with the complex structure of the ER has given rise to rapid evolutionary changes in the X-ray, optical, and mid-IR morphology of the emission. The Gemini South mid-IR images have established that the IR emission originates from dust in the ER that is swept up by the SN blast wave and collisionally heated by a soft X-ray component which has a temperature of 3.5×10^6 K and an ionization timescale of $n_e t \gtrsim 10^7$ cm^{-3} days. The *Spitzer* IR observations provide important complementary information on the evolution of the interaction of the SN blast wave with the ER and the properties of the dust in the hot X-ray-emitting gas. The results of our analysis are as follows.

1. *Spitzer* spectral observations on day 6190 after the explosion revealed that the dust consists of silicate dust grains radiating at an equilibrium temperature of $\sim 180^{+20}_{-15}$ K. Subsequent observations on day 7137 revealed that the IR flux increased by a factor of $\sim$2, with the dust composition and temperature remaining the same (Fig. 7).

2. The narrow range of grain temperatures constrains the range of grain sizes and the combinations of plasma temperature and densities capable of heating the dust to the observed range of temperatures. Using the X-ray constraint on the ionization timescale we limit the grain size distribution in the preshocked gas to be between 0.023 and 0.22 μm. The grain size distribution may have originally extended to smaller radii, but if so, these grains were evaporated by the initial UV flash from the SN.

3. The observed value of IRX, the IR-to-X-ray flux ratio is consistent with that expected from a dusty plasma with LMC abundances of heavy elements.

4. The value of IRX decreased by a factor of $\sim 0.53 \pm 0.16$ between days 6190 and 7137, suggesting that we are witnessing the effects of grain destruction on a dynamical timescale of the remnant. The magnitude of the decrease in IRX between the two epochs is strongly determined by the following factors: the grain size distribution in the preshocked gas of the ER; the density of the X-ray-emitting gas and the grain destruction efficiency; and the total time the dust is exposed to the flux of sputtering ions.

5. To follow the evolution of IRX, we constructed a model for the evolution of the grain size distribution in the shocked gas. In the model, pristine dust is continuously injected into the hot gas by the expanding SN blast wave and destroyed by thermal and kinetic sputtering behind the shock. The evolution of the grain size distribution resulting from the combined effect of dust injection and destruction is presented in Figure 5 for different geometries of the medium into which the blast wave is expanding.

6. The evolution in IRX represents the changes in the dust-to-gas mass ratio in the shocked gas resulting from grain destruction (see Figs. 6 and 9). Given the grain size distribution and plasma density, the decrease in IRX between two epochs can be used to determine the epoch at which the dust was first swept up by the SN blast wave. Conversely, knowledge of the epoch at which the SN blast wave first encounters the ER can be used to determine the grain destruction efficiency in the hot gas.

7. A self-consistent picture that emerges from the application of the model to the combined X-ray and IR observations is that of a SN blast wave expanding into a dusty fingerlike protrusion of the ER with a typical LMC dust-to-gas mass ratio. The dust in the preshocked gas consists of pure silicate dust with a normal LMC dust-to-gas mass ratio and a grain size distribution limited to radii between $\sim$0.023 and 0.22 μm, sufficiently large to stop the incident electrons. Smaller grain sizes may have formed in the mass outflow from the progenitor star, but were probably vaporized by the initial UV flash from the SN. The SN blast wave crashed into the ER between days 4000 and 6000 after the explosion giving rise to the observed soft X-ray emission. Typical temperatures and densities of the soft X-ray-emitting gas are $\sim 3 \times 10^6$ K and $(0.3-1) \times 10^4$ cm^{-3}, consistent with those required to collisionally heat the dust to a temperature of $\sim 180^{+20}_{-15}$ K. The plasma parameters and grain size distribution are consistent with the amount of grain destruction needed to account for the observed decrease in the IRX flux ratio between days 6190 and 7137. At these gas densities, the onset of grain destruction occurred about 1200–2000 days before the first *Spitzer* observations, consistent with the rise in the soft X-ray flux and the ionization time derived from X-ray models.

Further Gemini, ESO VLT, and *Spitzer* observations of SNR 1987A are in progress which, with combined X-ray observations, will shed further light on the nature of the morphology and dust properties of the circumstellar medium around the SN.

This work is based on observations made with the *Spitzer Space Telescope*, which is operated by the Jet Propulsion Laboratory, California Institute of Technology, under a contract with NASA. E. D. acknowledges partial support from *HST* grant GO 9114 for the Supernova INtensive Survey (SINS: Robert Kirshner, PI), and by NASA OSS LTSA 2003-0065. The work of R. G. A. was supported by a grant awarded to Spitzer Cycle 3 proposal ID 30067. R. D. G., E. F. P., and C. E. W. were supported by NASA through contract 1215746 issued by JPL/Caltech to the University of Minnesota. S. P. was supported in part by the SAO under *Chandra* grants GO 5-6073X and GO 6-7047X.

REFERENCES

Bouchet, P., De Buizer, J. M., Suntzeff, N. B., Danziger, I. J., Hayward, T. L., Telesco, C. M., & Packham, C. 2004, ApJ, 611, 394
Bouchet, P., et al. 2006, ApJ, 650, 212
Dwek, E. 1987, ApJ, 322, 812
Dwek, E., & Arendt, R. G. 1992, ARA&A, 30, 11
———. 2007, in AIP Conf. Proc. 937, Supernova 1987A, ed. S. Immler, K. Weiler, & R. McCray (New York: AIP), 58
Fischera, J., Tuffs, R. J., & Völk, H. J. 2002, A&A, 395, 189
Gehrz, R. D., & Ney, E. P. 1990, Proc. Natl. Acad. Sci., 87, 4354
Gehrz, R. D., et al. 2007, Rev. Sci. Instrum., 78, 011302
Houck, J. R., et al. 2004a, ApJS, 154, 18
———. 2004b, Proc. SPIE, 5487, 62
Iskef, H., Cunningham, J. W., & Watt, D. E. 1983, Phys. Medicine Biology, 28, 535
Lucy, L. B., Danziger, I. J., Gouiffes, C., & Bouchet, P. 1991, in Supernovae. Tenth Santa Cruz Workshop, ed. S. E. Woosley (New York: Springer), 82
Manchester, R. N., Gaensler, B. M., Staveley-Smith, L., Kesteven, M. J., & Tzioumis, A. K. 2005, ApJ, 628, L131
McCray, R. 2007, in AIP Conf. Proc. 937, Supernova 1987A, ed. S. Immler, K. Weiler, & R. McCray (New York: AIP), 3
Moseley, S. H., Dwek, E., Glaccum, W., Graham, J. R., & Loewenstein, R. F. 1989, Nature, 340, 697
Nozawa, T., Kozasa, T., & Habe, A. 2006, ApJ, 648, 435
Park, S., Burrows, D. N., Garmire, G. P., McCray, R., Racusin, J. L., & Zhekov, S. A. 2007, in AIP Conf. Proc. 937, Supernova 1987A, ed. S. Immler, K. Weiler, & R. McCray (New York: AIP), 43
Park, S., Zhekov, S. A., Burrows, D. N., & McCray, R. 2005, ApJ, 634, L73
Park, S., Zhekov, S. A., Burrows, D. N., Racusin, J. L., McCray, R., & Borkowski, K. J. 2006, in The X-ray Universe 2005, ed. A. Wilson (ESA SP-604; Noordwijk: ESA), 335
Polomski, E., Gehrz, R. D., Woodward, C. E., Boyer, M., & Roellig, T. L. 2004, BAAS, 36, 1466
Pun, C. S. J., et al. 2002, ApJ, 572, 906
Sugerman, B. E. K., Crotts, A. P. S., Kunkel, W. E., Heathcote, S. R., & Lawrence, S. S. 2005a, ApJ, 627, 888
———. 2005b, ApJS, 159, 60
Weingartner, J. C., & Draine, B. T. 2001, ApJ, 548, 296
Welty, D. E., Frisch, P. C., Sonneborn, G., & York, D. G. 1999, ApJ, 512, 636
Werner, M. W., et al. 2004, ApJS, 154, 1
Wooden, D. H., Rank, D. M., Bregman, J. D., Witeborn, F. C., Tielens, A. G. G. M., Cohen, M., Pinto, P. A., & Axelrod, T. S. 1993, ApJS, 88, 477
Yan, H., Lazarian, A., & Draine, B. T. 2004, ApJ, 616, 895
Zhekov, S. A., McCray, R., Borkowski, K. J., Burrows, D. N., & Park, S. 2006, ApJ, 645, 293
Zubko, V., Dwek, E., & Arendt, R. G. 2004, ApJS, 152, 211